UNIVERSITÀ DEGLI STUDI DI GENOVA FACOLTA'
DI MEDICINA E CHIRURGIA

BEYOND THE TIP OF THE ICEBERG IN MULTIPLE SCLEROSIS: THE ROLE OF OCT AND MRI IN DISEASE MONITORING

Tesi di Specializzazione
Scuola di Specialità in Neurologia

RELATRICE
Prof.ssa Matilde Inglese

CORRELATORE
Dott. Giacomo Boffa

CANDIDATO
Dott.Tommaso Sirito

Anno accademico 2023-2024

Summary

1. Background

1.1 Introduction

Multiple sclerosis (MS) is a chronic, inflammatory, demyelinating and neurodegenerative disease of the central nervous system (CNS). The pathological and radiological hallmark of the disease is the demyelinating lesion, which most commonly occurs in periventricular, juxtacortical, infratentorial, spinal cord region, or in the optic nerve. MS presents in 85% of cases with subacute-onset symptoms lasting at least 24 hours (referred to as a relapse). Relapses can manifest in various ways depending on the location and extent of the demyelinating lesions; the most common clinical presentations include optic neuritis, myelitis, cerebellar or brainstem syndromes, and cerebral hemispheric syndromes. In some cases, MS progresses slowly, with neurological decline occurring independently of relapses, a process referred to as disease progression. The clinical course of MS allows for the classification of the disease into distinct types. Historically, MS has been classified into three phenotypes, primarily based on the disease course. According to this classification, there is a relapsing-remitting form (RRMS), in which the main driver of disability is constituted by relapses in the absence of clinical progression between relapses. In contrast, when clinical progression occurs, either in the absence of relapses or between relapses, it can be classified as primary progressive MS (PPMS) if progression is present from disease onset, or secondary progressive MS (SPMS) if clinical progression develops after an initial relapsing-remitting phase[1].

RRMS typically manifests in the third and fourth decades of life, with a higher prevalence among females. As for the PPMS, the mean age of onset ranges from 39.5 to 64.3 years, with a slight female predominance[2 3].

Regarding the diagnosis, it is necessary, as per the 2017 McDonald criteria *(box 1)*, to demonstrate spatial and temporal dissemination of the disease. It is also mandatory to rule out other conditions that clinically and radiologically mimic MS. Notably, conditions that might enter the differential diagnosis include myelin oligodendrocyte glycoprotein antibody-associated disease (MOGAD),

neuromyelitis optica spectrum disorder (NMOSD), systemic autoimmune diseases with central nervous system involvement such as sarcoidosis or lupus, and monogenic vasculopathies like CADASIL.

BOX 1: The 2017 revised criteria for the diagnosis of MS[4]

Relapsing–remitting MS

- At least two clinical relapses and objective clinical evidence on neurological examination of at least two lesions with distinct anatomical location, or at least two clinical relapses and objective clinical evidence of one lesion and clear-cut historical evidence of a prior relapse involving a lesion in a distinct anatomic location
- At least two clinical relapses and objective clinical evidence of one lesion; in addition, DIS should be demonstrated by either a second clinical relapse implicating a different CNS site or using MRI[a]
- One clinical relapse and objective clinical evidence of two or more lesions; in addition, DIT should be demonstrated by a second clinical relapse, or using MRI[b] or demonstration of cerebrospinal fluid-specific OCBs
- One clinical relapse and objective clinical evidence of one lesion; in addition, DIS should be demonstrated by a second clinical relapse implicating a different CNS site or using MRI, whereas DIT should be demonstrated by a second clinical relapse, or using MRI or demonstration of cerebrospinal fluid-specific OCBs

Primary progressive MS

A disease course characterized by progression from onset, 1 year of disability progression (retrospectively or prospectively determined) independent of clinical relapse and two of the following criteria:

- One or more T2-hyperintense lesions in at least one area in the brain characteristic of MS (periventricular, cortical and/or juxtacortical or infratentorial)
- Two or more T2-hyperintense lesions in the spinal cord with no distinction between symptomatic or asymptomatic lesions
- Demonstration of cerebrospinal fluid-specific OCBs

CNS, central nervous system; DIS, dissemination in space; DIT, dissemination in time; MS, multiple sclerosis; OCB, oligoclonal band. [a]One or more T2-hyperintense lesions in at least two of four areas of the CNS (periventricular, juxtacortical (by combining cortical or juxtacortical lesions), infratentorial and spinal cord lesions), with the removal of the distinction between symptomatic and asymptomatic lesions. [b]Simultaneous presence of gadolinium-enhancing and non-enhancing lesions at any time, with the removal of the distinction between symptomatic and asymptomatic lesions, or a new T2-hyperintense and/or gadolinium-enhancing lesion on follow-up MRI with reference to a baseline scan irrespective of the timing of the baseline MRI.

It is therefore important for diagnosis, in addition to a thorough collection of medical history and a detailed neurological examination, to perform a brain MRI (or an MRI of the entire neuraxis). Other useful tests include lumbar puncture (to demonstrate the presence of oligoclonal bands), visual/motor, and somatosensory evoked potentials, to document functional alterations that cannot be identified using imaging techniques. Recently, new diagnostic criteria proposed in Copenhagen, at the 40th Congress of the European Committee for Treatment and Research in

Multiple Sclerosis (ECTRIMS) have paved the way for the use of advanced imaging techniques. In particular, it has been proposed:

- the involvement of the optic nerve, demonstrable through fundus oculi, visual evoked potentials, or OCT, as the fifth topography for spatial dissemination (DIS);
- Incorporating cerebrospinal fluid (CSF) kappa free light chain (kFLC) as a diagnostic biomarker, equivalent to CSF oligoclonal bands;
- Adding the central vein sign and paramagnetic rim lesion as imaging markers;
- Allowing a diagnosis of MS in patients with radiologically isolated syndrome (RIS) who fulfill spatial dissemination (DIS) criteria, even in the absence of clinical symptoms, provided they meet additional criteria such as temporal dissemination (DIT), presence of CSF biomarkers, or six or more central vein signs.

These criteria, among other objectives, aim to achieve earlier diagnosis and treatment.

The treatment for MS involves medications designed to modify the disease course, namely disease-modifying treatments (DMTs). These are divided into:

- **Low-efficacy therapies:** interferons, glatiramer acetate, teriflunomide, and dimethyl fumarate.
- **High-efficacy therapies:** more effective but generally associated with greater immunosuppressive effects, including natalizumab, anti-CD20 monoclonal antibodies, alemtuzumab, cladribine, and sphingosine-1-phosphate receptor modulators.

In cases where disease control is challenging despite the use of high-efficay treatment, autologous hematopoietic stem cell transplantation (AHSCT) may be considered. These therapies act in different ways on the immune system *(image 2)*. For instance, there are sequestering drugs that prevent immune cells from accessing the central nervous system (CNS), such as natalizumab and S1PR modulators. Additionally, there are depleting drugs (e.g., anti-CD20 monoclonal antibodies) and immune reconstitution therapies (IRTs), such as cladribine and alemtuzumab, which "reset" the immune system, rendering it less autoreactive.

Image 1: Cells, Molecules, and Therapies. This schematic provides a simplified overview of key cell types present in white-matter multiple sclerosis lesions, along with current and emerging therapeutic targets within the central nervous system and peripheral tissues[5].

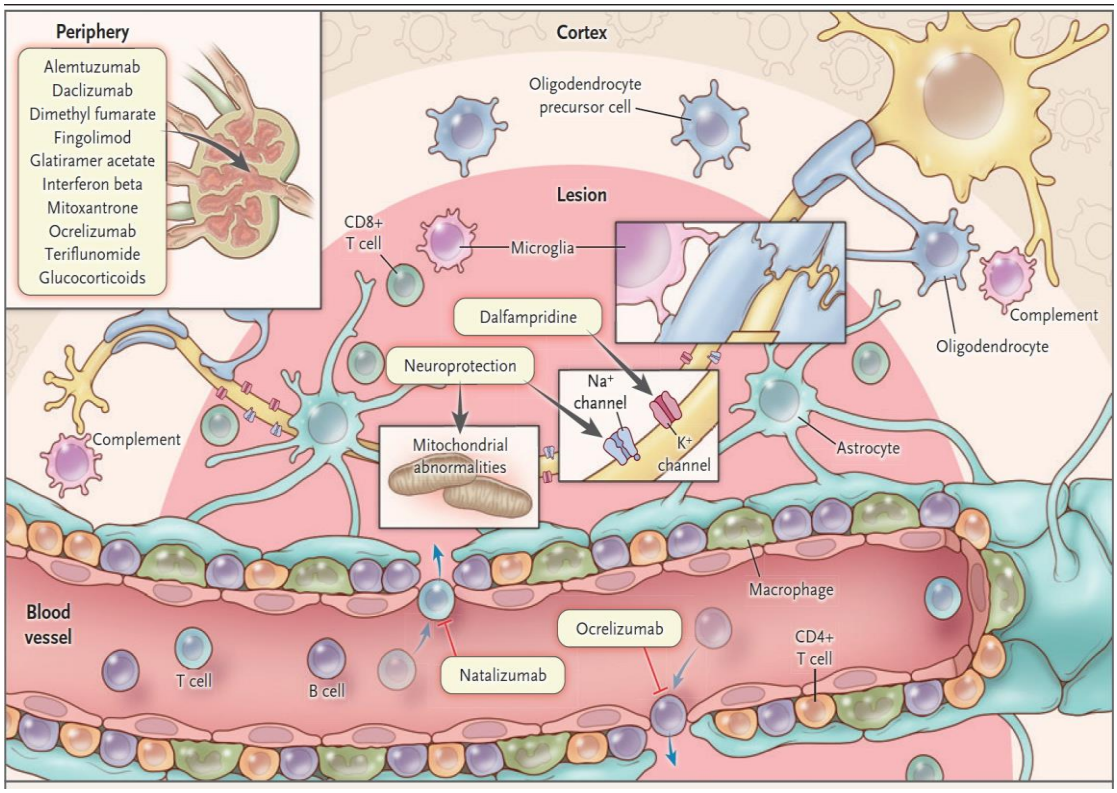

1.2 The paradigm shift in MS pathophysiology and its impact on treatment outcomes

The effective control of disease relapses—long considered the primary driver of disability—has brought to light another major contributor to disability: clinical progression, which stands as the true therapeutic challenge of recent years. Clinical progression is defined as an accumulation of disability measured by the Expanded Disability Status Scale (EDSS) in the absence of clinical relapses. Specifically, *confirmed disability progression* (CDP) is characterized by an increase in the EDSS score sustained over three months, with thresholds defined as follows: a 1.5-point increase if baseline EDSS is 0, a 1-point increase if baseline EDSS is between 1 and 5, and a 0.5-point increase if baseline EDSS is greater than 5[6].

The absence of CDP, along with the absence of clinical relapses and new MRI lesions, has been incorporated into the concept of NEDA-3 (No Evidence of Disease Activity), the most widely used and reproducible composite outcome in current clinical practice. However, the clinical reality is often more nuanced. Patients may report a worsening of symptoms—such as cognitive decline—that does not always correspond to a measurable deterioration in EDSS scores.

This scenario, characterized by a worsening of clinical symptoms that may or may not translate into EDSS changes, has prompted a paradigm shift in our understanding of the disease's pathophysiology. This shift involves moving from the traditional concept of focal cerebral inflammation, represented by demyelinating lesions, to the concept of *smouldering MS*[7]. According to this framework, the demyelinating lesion—the historical radiological and pathological hallmark of the disease—is the visible tip of the iceberg of a more widespread inflammatory process that affects even the seemingly healthy brain parenchyma, known as the *normal-appearing brain matter (NABM)*.

Moreover, it has been observed that the brain parenchyma and individual lesions exhibit varying capacities for remyelination. These differences are influenced not only by the natural aging process but also by interindividual variability. Consequently, the proportion of remyelinated lesions relative to non-remyelinated ones emerges as a strong determinant of disability.

Another fundamental mechanism from a pathophysiological perspective, and a significant driver of disability, is neurodegeneration. For a long time, this process was considered to be closely linked to the inflammatory aspects of the disease. However, emerging evidence over the past few years suggests that axonal injury and neurodegeneration may not be solely a consequence of demyelination[8].

Unfortunately, conventional imaging techniques, in addition to inadequately capturing pathological changes in NABM, also fail to accurately describe the evolution of lesions after their formation. Moreover, these methods are insufficient in precisely characterizing neurodegenerative processes. These aspects can be further investigated through advanced biomarkers—radiological, biohumoral, or neurophysiological—that can directly or indirectly document the various mechanisms of disease-related damage. The use of such biomarkers addresses the need for a multiparametric approach to MS, dictated by the inherent complexity of the condition.

1.3 Beyond the tip of the iceberg: the use of advanced MRI imaging

1.3.1 Insights into microstructural damage in the normal appearing brain parenchyma: the role of diffusion-weighted imaging

One such technique is undoubtedly diffusion-weighted imaging (dMRI). This method is based on metrics derived from the diffusion of water molecules which enable the evaluation of the brain's molecular function and microarchitecture. Indeed, the diffusion property refers to the ease with which water molecules move within biological tissues. In biological fluids, this movement is facilitated (which radiologically translates to "facilitated diffusion"), whereas in cellular structures, the movement is more restricted (resulting in "diffusion restriction"). One of the primary models used to analyze diffusion metrics in MS is Diffusion Tensor

Imaging (DTI). Among the key parameters extracted from DTI, we find Fractional Anisotropy (FA), which is particularly sensitive to axonal integrity, along with Axial Diffusivity (AD), and Radial Diffusivity (RD), Mean Diffusivity (MD), which characterize the direction of water molecules along three orthogonal planes within tissues. In demyelinating lesions and in the NAWM, an increase in MD, AD and RD is observed while FA is typically reduced[9].

Regarding FA, it is particularly useful for studying axonal damage in white matter, which is physiologically anisotropic. A reduction in FA, however, can also reflect other pathological processes, such as gliosis, cell death, or demyelination. Additionally, the characteristics of gray matter (GM), which is physiologically isotropic, make DTI less suitable for studying GM abnormalities. Such limitations of DTI highlight its reduced specificity when exploring the entire spectrum of brain abnormalities. On the other hand, Neurite Orientation Dispersion and Density Imaging (NODDI) is high specific and sensitive in detecting microstructural damage induced by pathology, even at the level of normal appearing gray matter (NAGM). While the DTI model relies on three orthogonal axes of diffusion, NODDI employs a three-compartment tissue model, which includes an intraaxonal compartment, namely Neurite Density Index (NDI), which reflect the density of neurites, an extra-neurite compartment, namely Orientation Dispersion Index (ODI), which quantifies the dispersion of neurite orientations and a water compartment, namely Isotropic Volume Fraction (ISOVF), typically associated with the extracellular space or non-neuronal tissue [10]. As for the NDI parameter, it is reduced both in lesions and in the NAWM of subjects with MS. Regarding ODI, however, the literature suggests an apparently 'artificial' reduction in demyelinating lesions, likely reflecting a decreased signal generated by destroyed nerve fibers rather than a true reduction in dispersion, while it is increased in the NAWM[9].

The NODDI model has proven to be more specific and sensitive than the DTI model in defining the microstructural damage caused by the pathology. Indeed, some studies suggest that NODDI metrics detect damage in regions where FA values remain normal[11]. This highlights its growing use as a diffusion model and a potential outcome measure in research settings and, in the future, clinical practice. For instance, in a study by Granberg et al.[12], a greater reduction in NDI was observed in patients with secondary-progressive MS compared to those with relapsing-remitting MS, suggesting the potential role of this model in patient

phenotyping. However, other studies have reported no statistically significant differences in NDI within demyelinating lesions and NAWM between relapsing-remitting MS (RRMS) and primary-progressive MS (PPMS) patients[13].

Nevertheless, NODDI remains highly valuable as its metrics correlate with other unconventional parameters and biomarkers of the disease, such as cognitive test performance[14], offering a multiparametric approach to understanding MS. Additionally, NODDI can be used to study axonal integrity in specific pathways, such as the visual one, and it would therefore be essential for a better pathophysiological insight into the damage observed on OCT.

1.3.2 Insights into neurodegeneration: the role of atrophy quantification

Cerebral volume loss is a physiological mechanism that increases with age. Studies have shown that brain volume decreases range from –0.05% per year in individuals aged 20–30 to –0.3% per year in those aged 60–70[15]. However, an accelerated global brain volume loss is now recognized as a pathological marker of MS. A change of –0.4% per year has been proposed as the cut-off for pathological brain atrophy in MS[16], although caution is required before adopting this threshold as a marker of therapeutic efficacy, due to the confounding phenomenon of pseudoatrophy[17]. This loss of brain volume, in addition to being a potential consequence of focal inflammatory processes, can also represent the epiphenomenon of a global neurodegenerative process. Such a process encompasses the pathophysiological mechanisms of neuronal loss, axonal degeneration, astrocytic damage, and meningeal inflammation, which affect not only demyelinating lesions but also normal-appearing brain parenchyma (NABP). The brain volume loss, which acts as a significant driver of disability accumulation independent of relapses, is also observed, although with a cause-effect relationship not yet well elucidate, in patients with relapsing-remitting MS[18].

Indeed, a 2020 MAGNIMS consensus recommends the use of this biomarker across all disease phenotypes, including during the early stages, due to its significant predictive value[19].

Additionally, spinal cord atrophy, particularly at the cervical level, has been identified as a critical biomarker of disability. Notably, cervical spinal cord atrophy exhibits greater accuracy than brain volume loss in distinguishing patients with a

relapsing-remitting phenotype from those with progressive forms[20]. Furthermore, a correlation has been demonstrated between spinal cord atrophy and retinal nerve fiber layer (RNFL) thinning[21].

The pathological and clinical significance of brain volume loss is such that this metric has been incorporated into the NEDA-4 concept as a composite efficacy outcome[22]. Numerous clinical trials have employed brain volume loss as an outcome measure. This is justified not only by the clinical impact of atrophy but also by the high reproducibility of results and the increasing availability of fully automated pipelines for brain volume quantification, such as SIENAX and FreeSurfer.

Brain atrophy is, therefore, one of the most promising markers for potential introduction into clinical practice. Furthermore, its correlation with other disease parameters, such as retinal layer thinning observed through OCT, may provide additional insights into its pathological significance.

1.3.3 The role of quantitative susceptibility mapping (QSM) in defining lesion phenotypes in MS

As previously mentioned, an important determinant of disability is the central nervous system's ability to repair damage through remyelination, as well as the behavior of demyelinating lesions, not only during the acute phase but also over time. It is now well-established that after the acute phase of inflammatory demyelination at lesion onset, chronic lesions can exhibit different pathological and repair outcomes, which significantly impact the patient's clinical prognosis.

Several studies have sought to clearly define the progression of demyelinating lesions. The currently recognized histological classification categorizes lesions as active and demyelinating, active and post-demyelinating, mixed active/inactive and demyelinating, mixed active/inactive and post-demyelinating, and inactive. This classification reflects the temporal evolution of lesions based on the distribution of macrophages/microglia containing or lacking myelin degradation products.

Histologically, demyelinating lesions are characterized by macrophages/microglia containing myelin degradation products, unlike post-demyelinating lesions, which contain macrophages/microglia without myelin degradation products. Active

lesions display a uniform distribution of macrophages/microglia throughout the lesion, whereas in mixed active/inactive lesions, macrophages/microglia are confined to the lesion's periphery[23]. Inactive lesions exhibit little to no inflammatory content.

This complex histological classification deliberately excludes the remyelination process, as remyelination is a dynamic mechanism that can occur at any stage in the biological history of a lesion. Remyelination, long debated, is now recognized as a well-established repair mechanism that is variably present among patients with MS[24].

There have been numerous attempts to translate the intricate histological framework described above into more accessible biomarkers. One promising approach involves magnetic resonance techniques, such as phase imaging and quantitative susceptibility mapping (QSM), which are sensitive to iron. Iron, being paramagnetic and hyperintense on QSM, can be used to localize macrophages within lesions and thus reflect their histological characteristics.

QSM also allows for the identification of myelin as a diamagnetic substance due to its lipid content, which appears hypointense on susceptibility maps. The contrasting properties of iron and myelin are leveraged to radiologically classify demyelinating lesion subtypes as follows:

- **Paramagnetic rim lesions**: hypointense lesions with a hyperintense rim corresponding to the presence of macrophages/microglia containing iron. These lesions serve as biomarkers of mixed active/inactive lesions (or, as described by some authors, chronic active/smouldering lesions), as previously discussed.
- **Hypointense or isointense lesions**: these are classically defined as remyelinated lesions;
- **Globally hyperintense lesions**: suggested by some authors as markers of chronic inactive lesions.

However, the opposing signals provided by iron and myelin complicate the pathological interpretation of globally hyperintense lesions. These lesions may reflect either low myelin content or high iron deposition. This challenge could be addressed through the use of techniques such as χ-separation, which generate

distinct maps for paramagnetic and diamagnetic signals, allowing for more precise characterization.

Additionally, the identification of paramagnetic rim lesions currently requires manual delineation by an operator, reducing the objectivity of the assessment, as no automated tools capable of reliably detecting these lesions are currently available. Despite this limitation, the diagnostic significance and specificity of paramagnetic rim lesions[25] have led to their inclusion in the updated diagnostic criteria proposed at the ECTRIMS conference held in Copenhagen in 2024.

From a prognostic perspective, paramagnetic rim lesions hold substantial importance. Patients with multiple chronic active lesions exhibit more aggressive disease phenotypes, characterized by higher lesion load, reduced white matter and basal ganglia volumes, and greater motor and cognitive disability. These patients are also more likely to transition to progressive course[26]. This supports the view of some authors who advocate prioritizing lesion phenotyping over lesion quantity. However, given the subjective nature of QSM assessment and the unclear clinical and pathological significance of hyperintense lesions, integration with other biomarkers, such as OCT, is still necessary.

1.4. Beyond the tip of the iceberg: the role of OCT

1.4.1 Introduction to OCT and pathophysiological insights

Optical coherence tomography (OCT) is a non-invasive, fast, and cost-effective imaging technique that uses near-infrared light to generate high-resolution and reproducible images of retinal layers[27], both at the macula and at the optic nerve head. One of the reasons to study the visual pathway in individuals with MS is its clinical significance. Visual symptoms are indeed common in MS, with optic neuritis (ON) being the onset symptom in approximately 20% of patients. The significance of this is such that optic nerve involvement, detectable through OCT, fundus examination, MRI, or visual evoked potentials, has been included in the new diagnostic criteria presented in Copenhagen.

The retina is a multi-layered structure crucial for visual processing, with each layer serving a unique role. The most studied layers in MS are the Retinal Nerve Fiber Layer (RNFL), the Ganglion Cell Layer (GCL), the Inner Plexiform Layer (IPL),

and the Inner Nuclear Layer (INL) *(image 2)*. IPL is a site of synaptic connections crucial for signal integration; INL contains the cell bodies of bipolar, horizontal, and amacrine cells involved in visual signal refinement. In the GCL and in the RNFL, respectively, the somas and axons of the retinal ganglion cells are located. The thickness of the RNFL is usually measured at the peripapillary level, while the thickness of the other layers is measured at the macular level.

The axons originating from the RNFL, initially unmyelinated, form the optic nerve. After passing through the lamina cribrosa, the optic nerve acquires its myelin sheath. It travels through the optic canal until it reaches the optic chiasm, where the nasal fibers decussate, while the temporal fibers continue on the same side. Subsequently, through the optic tract, these fibers reach the lateral geniculate nucleus, where they synapse with the dendrites of neurons. The axons of these neurons then form the geniculocalcarine tract (or optic radiation), which carries visual information to the primary visual cortex.

The initial OCT devices utilized time-domain technology (TD-OCT), which was capable of measuring the thickness of the peripapillary RNFL (pRNFL). Consequently, this layer became the primary focus of early research. Indeed, the first use of RNFL thickness measurement in individuals with MS dates back to 1999, when a study demonstrated, unsurprisingly, that RNFL values were lower in the eyes of patients who had experienced ON at least one year prior, compared to healthy controls[28]. Since then, OCT has been increasingly employed to objectively and reproducibly quantify the damage caused by previous episodes of optic neuritis. We now know with certainty that the thinning of the RNFL following ON is a manifestation of retrograde axonal degeneration.

In reality, it has been known for several years that ON is not the only mechanism of damage to the optic nerve. In 1976, autopsy studies were published documenting the presence of changes in the optic nerves of individuals without a previous history of optic neuritis[29], suggesting the presence of a more complex damage mechanism.

Subsequently, the introduction of spectral-domain OCT (SD-OCT) technology enabled the assessment of additional retinal layers, including the macular mRNFL,

ganglion cell layer (GCL), inner plexiform layer (IPL), inner nuclear layer (INL), outer plexiform layer (OPL), and outer nuclear layer (ONL).

The ability to study the thickness of the GCL, which contains cell bodies, and other retinal layers, along with the integration of increasingly advanced MRI data, has allowed the proposal of new mechanisms of damage. Some authors, for example, have suggested a primary degeneration of the cell bodies in the GCL induced by the disease. Others, however, have proposed a retrograde trans-synaptic axonal degeneration mechanism. Particularly, as we will see, various studies have correlated damage in a segment of the retrochiasmatic visual pathway with damage observed on OCT. However, defining a correlation does not necessarily establish the "primum movens". Therefore, in patients without a prior history of ON, it remains unclear in which direction trans-synaptic degeneration occurs. In contrast, in patients with a history of ON, a mechanism of Wallerian degeneration can be hypothesized, given the findings in several studies that correlate ON with, for example, neuronal depletion at the lateral geniculate body[30] and structural disorganization along the optic radiation[31].

However, for this mechanism of damage propagation, OCT, a simple and non-invasive examination, is considered as a window into the visual pathway, which is relatively easy to study. In fact, other studies have highlighted a correlation between retinal thinning and MRI parameters not exclusively related to the visual pathway, such as white matter and gray matter global atrophy, lesion burden and number and volume of cortical lesions[27].

Several aspects remain to be defined regarding the role of OCT in MS. Does it merely reflect a mechanism of focal retrograde axonal degeneration, or does it indicate a more global process? Furthermore, which pathological mechanism of the disease does it best represent? Is it more closely associated with focal inflammation, smouldering MS, or neurodegeneration?

These questions highlight the complexity of interpreting OCT findings and their relationship with the broader pathophysiological landscape of MS.

Image 2: Visualization of Retinal Layers at the Macular Level Using OCT [32]

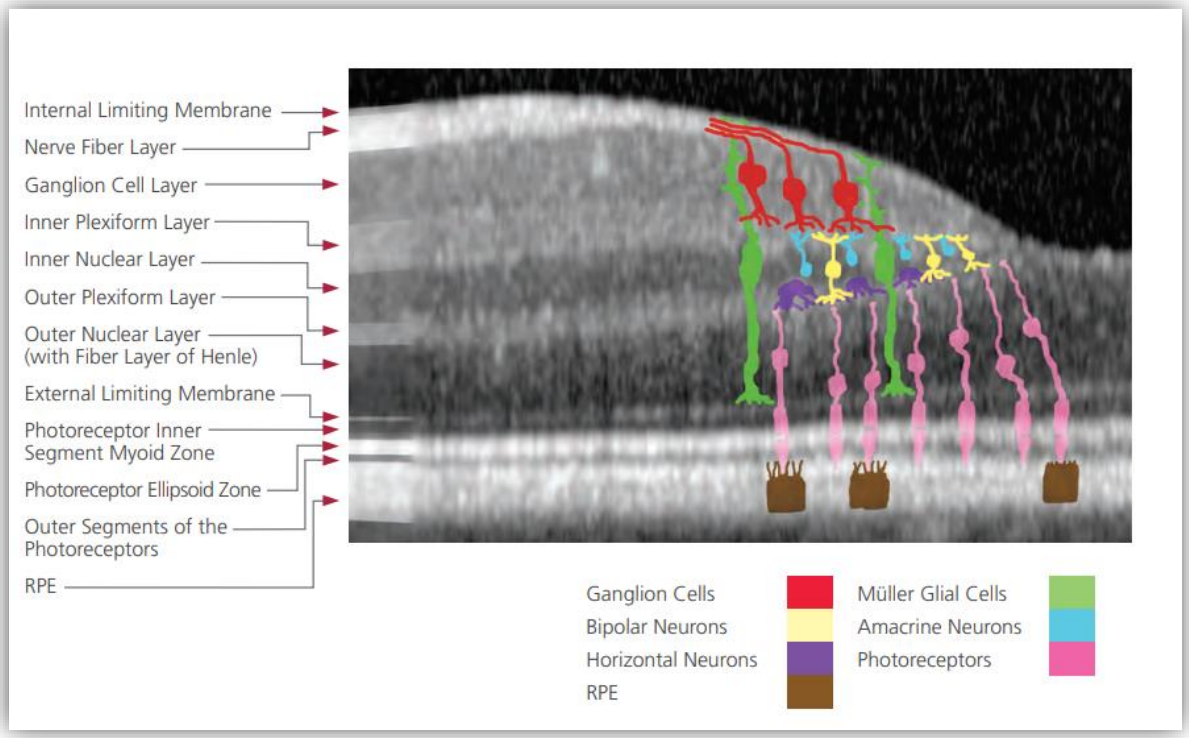

As previously mentioned, the thinning of RNFL as well as GCIPL, can objectively detect the effects of a prior episode of optic neuritis (ON). The objectivity of this assessment not only allows for precise long-term follow-up but also aids in excluding non-organic causes of unilateral visual disturbances, such as psychosomatic disorders.

It is now well established that following an episode of optic neuritis, GCIPL thinning occurs earlier than RNFL thinning. This is likely due to the more significant edematous process affecting the RNFL. Studies suggest that RNFL thinning begins between 2 and 6 months post-ON and stabilizes around 7 to 12 months[33]. In contrast, GCIPL thinning is detectable much earlier, occurring within the first few weeks after the event[34].

However, it is generally recommended to perform OCT at least 3 months after an episode of optic neuritis to ensure reliable detection of structural changes.

Moreover, OCT represents a valuable tool in the differential diagnosis of conditions that mimic MS, such as Neuromyelitis Optica Spectrum Disorder

(NMOSD). In patients with MS and a history of ON, RNFL thinning is less pronounced and predominantly affects the temporal sector. In contrast, in patients with NMOSD and a history of ON, RNFL thinning is more severe and involves all sectors, particularly the superior and inferior sectors.

RNFL thinning in MS also occurs subclinically, a phenomenon that is not observed in NMOSD. Furthermore, NMOSD shows significant involvement of the GCL, especially in the superior sector, due to the expression of AQP4 by Müller cells and retinal astrocytes. Notably, GCL thinning in NMOSD, unlike RNFL thinning, can occur subclinically, challenging the notion of an exclusively inflammatory or subacute nature of the disease[35], therefore suggesting a neurodegenerative astrocytopathy. Moreover, microcystic macular edema at the level of the inner nuclear layer occur at a higher frequency in NMOSD than in MS after ON (~21% versus ~5%)[36].

Significant involvement of the superior sector of the GCL is also observed in a condition that can mimic inflammatory optic neuritis: anterior ischemic optic neuropathy. In such cases, the use of OCT angiography is essential to document vascular damage.

In patients non arteritic anterior ischemic optic neuropathy (NAAION), as in patients with Susac syndrome[37], retinal involvement is patchy, reflecting an ischemic process localized to specific retinal areas. Conversely, in patients with arteritic anterior ischemic optic neuropathy (AAION), the process is more diffuse.

Regarding the distinction between Myelin Oligodendrocyte Glycoprotein Antibody Disease (MOGAD) and MS, peripapillary RNFL thinning is more pronounced in MOGAD than in MS, while no significant differences are observed in macular measurements[38].

Moreover, OCT has been shown to correlate with clinical measures. For instance, several studies demonstrate a correlation between the EDSS and the thinning of the GCIPL and pRFNL[39]. In addition, significant correlations have been found between GCIPL/RNFL thickness and visual acuity, particularly low-contrast visual acuity[40 41], as well as between GCIPL thickness and dyschromatopsia[42]. Furthermore, GCIPL has been associated with gait speed[43]. OCT findings in retinal layers have also been linked to cognitive outcomes, including cognitive

processing speed, verbal learning and memory, visual learning and memory, and verbal fluency[44,45].

Additionally, OCT measures of both RNFL and GCIPL thickness have been suggested as potential predictors of disability progression over the following years. In particular, Martínez-Lapiscina et al. on behalf of the IMSVISUAL consortium showed in more than 800 patients with MS an association of thinned pRNFL ≤87 μm with disability accrual after 3 years measured by expanded disability status scale (EDSS)[46]. More recently, Rothman et al. published a study showing that lower baseline TMV measured by OCT significantly predicts higher disability at 10 years, even after accounting for baseline disability status[47]. Furthermore, Zimmermann and Knier et al. showed thinner GCIPL values to be predictive for the violation of the "no evidence of disease activity" (NEDA) criteria in patients with CIS defined by (1) new attacks or (2) disability accrual measured by EDSS or (3) enlarged or new MRI lesions[48].

OCT has also proven useful in patient phenotyping and distinguishing between relapsing-remitting (RR), primary progressive (PP), and secondary progressive (SP) forms of MS. Specifically, studies have shown that patients with SPMS exhibit more pronounced thinning of the RNFL, GCIPL, and TMV compared to those with RRMS. However, these differences are more pronounced in the GCIPL[41] and in eyes unaffected by prior optic neuritis, as in such cases, the influence of optic neuritis predominates over the effects of neurodegeneration[49].

In PPMS, retinal layer thickness is consistently reported to be reduced compared to RRMS, provided there is no history of prior optic neuritis. There has been ongoing debate regarding the role of OCT in differentiating PP from SP forms of MS. While no significant differences in TMV have been observed in literature[50]—reflecting a shared neurodegenerative component between the two forms—SP patients exhibit more RNFL thinning compared to PP patients[51]. This finding may reflect a greater involvement of the visual pathway in SP MS.

Moreover, the use of OCT, due to its ease of execution and its ability to capture various aspects of the pathology, has frequently been employed to assess the efficacy of treatments and to define outcomes. In fact, it has been observed that

there is a correlation between the effectiveness of disease-modifying therapies and the reduction of retinal thinning processes[52].

These facts have supported the increasingly frequent use of OCT, both in clinical practice and clinical trials, as a marker of treatment efficacy.

1.4.3 Integrating OCT and MRI biomarkers

Given the evident ability of OCT to reflect various aspects of the pathology, numerous studies have investigated the correlation between this biomarker and neuroradiological markers. Among the most commonly used radiological biomarkers is brain atrophy. In 2007, the first study was published describing a strong correlation between pRNFL thickness and MRI-derived brain parenchymal fraction as a marker of brain atrophy. Since then, a plethora of studies has examined the association between greater brain atrophy and thinning of various OCT layers.

While the correlation between brain atrophy and thinning of the retinal layers is well established, some aspects of this association remain debated. For instance, conflicting results have emerged regarding which of the two layers, RNFL or GCIPL, is better able to reflect brain atrophy. A study by Vidal-Jordana et al. demonstrated a cross-sectional correlation between reduced pRNFL thickness and GCIPL volume with brain parenchymal fraction, gray matter fraction, and spinal cord area[39]. Conversely, another study highlighted a strong association between grey matter, white matter, and thalamic atrophy with GCIPL, downplaying the role of pRNFL in reflecting cerebral atrophy[53].

A study by Cagol et al.[54] further explored these relationships, showing that in PwMS, both pRNFL and GCIPL were positively associated with total brain volume and total grey matter volume, but not with total white matter volume (*image 3)*.

Notably, the same study also highlighted the correlation between OCT thinning and regional cortical volumes, with no significant difference observed in the strength of the association between the occipital cortex and OCT compared to other cortical regions. In this context, another major dilemma in the field is whether OCT serves

as a window into a global neurodegenerative process or is merely an expression of a “focal” retrograde degeneration. It is now well established that damage to the optic radiation, whether in terms of structural disorganization or demyelinating lesions, can lead to OCT thinning. However, the underlying reasons for the association between global neurodegeneration and retinal damage remain unclear.

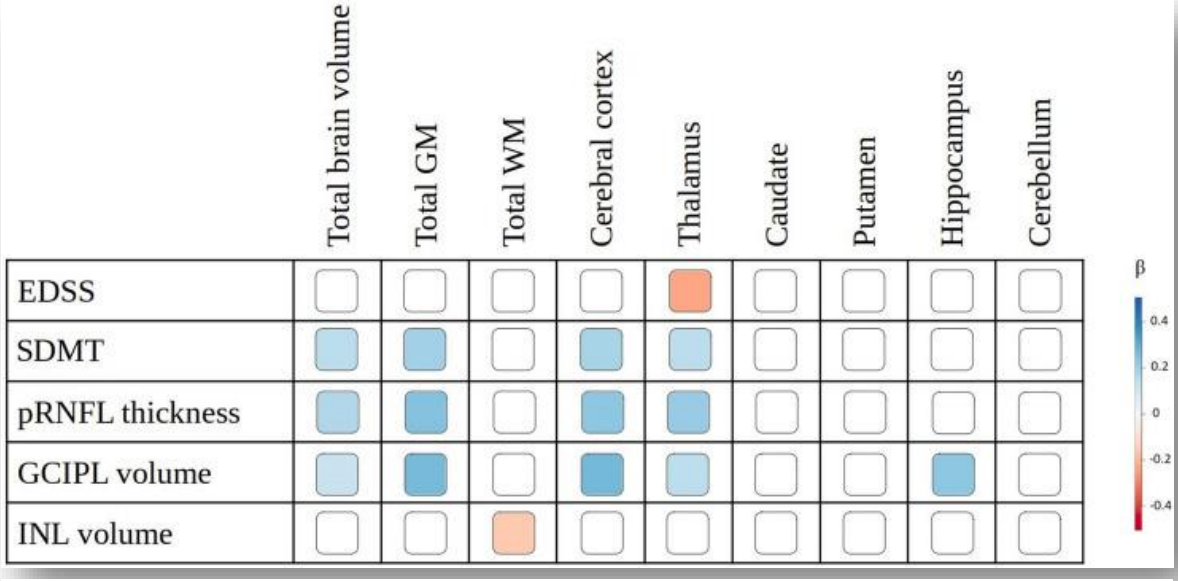

Image 3: associations between MRI measures, OCT measures, and disability measures in the study by Cagol et al. The effect size, expressed as standardized beta(β), is graphically displayed for each brain volume that shows a significant association

Intriguing, albeit contrasting, results have emerged from studies on pathologies with a predominantly neurodegenerative component, where the confounding factor of demyelination is absent, such as tauopathies. For instance, one study demonstrates a correlation between occipital and temporal atrophy and OCT thinning[55]. Another study highlights the challenges of using OCT in the differential diagnosis between Alzheimer's disease and other neurodegenerative conditions with greater posterior involvement[56], such as Lewy body disease.

These studies highlight the challenge of defining the relationship between global neurodegeneration and damage to the optic nerve.

Another poorly elucidated aspect of optic nerve damage in MS is its association with another driver of disability: chronic active inflammation. In this context, a study by Kranjc et al. [57] demonstrated the predictive value of the number of paramagnetic rim lesions (PRLs) on future thinning of the RNFL and GCIPL.

Nevertheless, the questions we raised earlier regarding the precise pathophysiological significance of retinal layer thinning remain unanswered to this day. Understanding the interplay between retinal changes, chronic active inflammation, and global neurodegeneration requires further investigation, emphasizing the need for a multiparametric approach to disentangle these complex mechanisms.

2. Introduction to the experimental part

The integration of OCT with neuroradiological data is therefore crucial in a research setting to define the etiology and damage mechanisms in MS. In clinical settings, the integration of biomarkers is equally important for assessing patient outcomes through a multiparametric approach, allowing for a more comprehensive understanding of disease progression and treatment efficacy.

The concept of "efficacy" has evolved alongside the paradigm shift in the pathophysiological understanding of MS. As previously discussed, critical mechanisms such as smouldering MS and neurodegeneration, which clinically manifest as progression independent of relapse activity (PIRA), can occur independently of the formation of new demyelinating lesions. These mechanisms can emerge even in patients with a relapsing-remitting phenotype and in the early stages of the disease. In this context, the early initiation of disease-modifying therapy (DMT) has been shown to correlate with better prognosis, not only in the short term but also in the long term[58]. This highlights the necessity of incorporating the speed of action into the definition of a treatment's efficacy.

Advanced MRI techniques, such as neurite orientation dispersion and density imaging (NODDI), can aid in this effort by providing near in vivo assessment of the structural damage caused by the disease.

In the present research project we wanted to:

1) evaluate, through a multiparametric approach. the efficacy and speed of action of two drugs with different pharmacodynamic profiles: fingolimod, a lymphocyte sequestering agent, and cladribine, an antimetabolite;
2) characterize a cohort of patients treated with ocrelizumab through the assessment of brain and retinal volumes over 24 months. Additionally, we sought to further elucidate the role of OCT by investigating correlations between pRNFL and GCIPL thicknesses and chronic active lesions

3. First axis: Evaluating the rapid suppression of inflammation induced by fingolimod and cladribine: a combined clinical, OCT and MRI approach

3.1 Material and methods

3.1.1 Study design

This is a prospective, longitudinal, real-world study. Sixty-five patients who were prescribed treatment with either fingolimod (n=32) or cladribine (n=33) were enrolled. Inclusion criteria were: (i) age 10-70 years (ii) MS diagnosis according to the 2017 McDonald's criteria[59]. Exclusion criteria were: (i) contraindications to MRI, (ii) progressive disease course according to Lublin's criteria[1]. Patients were clinically evaluated every 3 months for assessment of effectiveness and safety. Sixty-four (98%) underwent baseline and 12-months follow-up (FU) MRI scans at our institution with a standardized 3T MRI protocol (Siemens PRISMA).

53 patients underwent spectral domain optical coherence tomography (SD-OCT) at the same timepoints.

3.1.2 Clinical assessment

Clinical evaluation included (a) assessment of Extended Disability Status Scale (EDSS) score[60]; (b) Nine-Hole Peg Test (9-HPT)[61]; (c) Timed 25-foot walk test[62]; and (d) NIH Toolbox Standing Balance Test[63]. The NIH Toolbox Standing Balance Test is a tool that assesses balance maintenance in five positions: with open and closed eyes on solid and soft surfaces and with open eyes in a tandem position on a solid surface. A coefficient is calculated based on the patient's balance during each position; the average of the 5 coefficients, known as the theta value (ranging from -2 to +2, where a lower value indicates less balance in the patient), is a reliable and validated estimate of the patient's balance. Information regarding occurrence of clinical relapses and/or disability progression during FU were collected.

3.1.3 MRI acquisition and processing

MRI exam was performed using a 3-T Siemens MAGNETOM Prisma (Siemens Healthcare, Erlangen, Germany) scanner with a 64-channel head and neck coil. The MRI protocol included:

(i) 3D sagittal T2- FLAIR (repetition time/inversion time/echo time (TR/TI/TE): 5000 ms/1800 ms/393 ms; resolution 0.4 × 0.4 × 1 mm 3, acquisition time 6min37");

(ii) (ii) 3D sagittal T1 MPRAGE (TR/TI/TE: 2300 ms/919 ms/2.96 ms;resolution 1 × 1 × 1 mm 3 , acquisition time 5min12");

(iii) (iii) twice-refocused spin echo echo-planar imaging sequence for diffusion MRI with 108 directions distributed in 5 shells with b-value up to 3000s/mm², in addition to seven b = 0 images (TR/TE: 4600/75 ms, flip angle 90°, spatial resolution 1.8 × 1.8 × 1.8 mm3, acquisition time 10min10"). Seven b = 0 image volumes with reversed phase-encoding direction were also acquired to correct for susceptibility-induced image distortions.

Of the 65 patients who underwent standardized 3-T MRI, 5 patients were excluded from the analyses of advanced resonance measurements due to: (I) treatment discontinuation within 6 months from treatment start (n=2; 1 patient in the fingolimod and 1 in the cladribine group); (II) poor quality (n=3, 2 patients in the fingolimod group and 1 in the cladribine group). Accordingly, MRI data were available for 31 patients treated with cladribine and for 29 fingolimod treated patients. Information regarding the presence of radiological disease activity (new/enlarging FLAIR lesions and gadolinium enhancing lesions) during FU was collected.

As for the processing of lesion segmentation, lesions with T2 hyperintensity and T1 hypointensity were identified and delineated on FLAIR and T1-weighted images, respectively using a semi-automated segmentation technique based on user-guided local thresholding within a web-based platform (SinLab, SienaImaging, Siena, Italy; https://sinlab-rhb.sienaimaging.com). Subsequently, the corresponding T1 images were adjusted using the T1-hypointense lesion mask and the FMRIB Software Library (FSL) (Oxford, UK; https://fsl.fmrib.ox.ac.uk). As for the

processing of brain atrophy, normalized brain, white matter (WM), and gray matter (GM) volumes were obtained through a fully automated segmentation pipeline (CAT12)[64]. To ensure quality, all segmentation maps underwent a meticulous review process conducted by the same two expert neurologists. Changes in percentage-brain-volume- change (PBVC) were measured.

For the processing of diffusion MRI data, initial denoising was carried out using the Marchenko-Pastur principal component analysis algorithm available in Mrtrix3[65]. Subsequently, corrections for motion artifacts and susceptibility-induced distortions were applied using the 'eddy' and 'top-up' commands from FSL. As a final pre-processing step, B1 field inhomogeneity correction was applied to all diffusion MRI volumes using the ANTs N4 algorithm. The NODDI model was applied to extract the Intra-Cellular Volume Fraction (ICVF) and Orientation Dispersion (ODI). The first measures the volume occupied by cellular structures in brain tissue. The second quantifies the dispersion of neural fiber orientations in a brain region, indicating how fibers align or spread[66]. The Corpus Callosum (CC) region of interest (ROI) for the was extracted from the JHU atlas[67]: a non-linear transformation (Symmetric normalization, which combines an Affine and deformable transformation) was used to register the T2 image based on JHU template onto the mean b=0 volume extracted from the dMRI images[68].Then the resulting transformations were applied to register the CC ROI within the dMRI space. Moreover, the coregistered CC mask was eroded by one voxel to avoid Partial Volume Effect (PVE) with neighboring tissue. All the registrations underwent visual inspection for quality assurance. Finally, the mean values of diffusion microstructural maps were extracted within the CC mask.

3.1.4 OCT

Standardized spectral-domain-OCT protocols (Spectralis, Heidelberg-Engineering) were performed and processed by a single certified neurologist, in accordance with the APOSTEL recommendations [69]. Peripapillary retinal nerve fiber layer (pRNFL) was obtained with a 360° RNFL-B circle scan located at 3.4 cm from the center of the optic nerve head; peripapillary measurements were averaged from 100 images and macular estimations from 15 ART. Macular volumetric scans consisting of at least 25 single horizontal axial B-scans were acquired in a rectangular section centered over the macula and segmented automatically into different layers using

the Heidelberg Eye Explorer mapping software version 6.0.9.0. Segmented layers were checked and manually corrected, if necessary. The combined thickness of ganglion cell layer + inner plexiform layer (GCIPL) was measured. Scans violating international-consensus quality-control criteria (OSCAR-IB)[70] were excluded (n=8 fingolimod treated and n=6 cladribine treated patients excluded due to poor OCT quality). Patients with previous bilateral optic neuritis (ON) were excluded (n=4). In patients with previous unilateral ON (n=44, none occurring during the previous 12-months), only the non-affected eye was analyzed. In patients without history of ON, OCT metrics were averaged over the two eyes.

3.1.5 Study endpoints

The endpoints of our study were to compare the: I) percentage of patients free from clinical relapses, MRI activity and disability progression (according to the NEDA-3 definition) during the first 12 months after treatment start; II) changes in 9-HPT, T25-foot walk, and theta value at NIH Toolbox Standing Balance Test scores; (III) percentage of patients maintaining NEDA-4 (NEDA-3 plus absence of pathological brain atrophy, defined as an annualized PBVC>-0.4%[16]); (IV) retinal (pRNFL and GCIPL) atrophy; (V) changes in NODDI metrics (ODI and ICVF) within the corpus callosum.

3.1.6 Statistical analyses

Statistical analyses were performed with SPSS (v26.0) and Jamovi (v 2.5.2.0). Descriptive results were reported as mean with standard deviation (SD) or median with interquartile range (IQR). Demographic differences between groups were analyzed using Chi-square, Mann-Whitney and Student's t-test when appropriate. The probability of disability worsening-free survival, relapse-free survival, MRI activity-free survival, and NEDA-3 status was calculated with the Kaplan–Meier estimator. Differences in terms of clinical (9-HPT, T25-foot walk and theta value at NIH Toolbox balance standing test scores), MRI (T2 lesion load, ODI and ICVF of

CC) and OCT (pRNFL and GCIPL) metrics at different timepoints were assessed with repeated-measure analysis of covariance, adjusting for age, sex, and disease duration. A two-sided $p < 0.05$ was used for statistical significance.

3.2 Results

3.2.1 Study population

Patients were well balanced for main baseline characteristics. Mean age at baseline was 39.4 (SD +/- 11.3) years in the cladribine-treated group (CLAD) and 40.1 years (SD +/- 16.7) in the fingolimod-treated group (FINGO), with 66.7% and 62.5% of females, respectively. Mean disease duration was 7.7 (SD +/- 9.2) and 9.4 (SD +/-10) years for CLAD and FINGO respectively, with a median EDSS at baseline of 1.5 (with a range of 0-4.5 for CLAD group and 0-5.5 for FINGO group) for both groups. 39.4% of patients who initiated CLAD had MRI activity at baseline vs 62.5% of those who initiated FINGO (p=0.06).

3.2.2 Outcomes

After 12 months, 81.8% of CLAD patients obtained NEDA-3 status compared to 71.9% of FINGO patients (p=0.41) (figure 1). Only one patient treated with fingolimod had disability progression, which was independent of relapse activity. The percentage of patients free of relapse activity was 93.9% and 100%, for CLAD and FINGO respectively. Two patients relapsed under CLAD (one had a relapse 3 days after the start of therapy -with subsequent persistent MRI activity-, while the other relapsed after 258 days). 81.8% of CLAD patients was free of MRI activity versus 75%, in the FINGO group. Mean time to MRI activity was 160 days and 229 days, respectively.

CLAD patients exhibited a minimal increase of 0.45 seconds (SD +/- 3.21) in T25FW compared to 1.07 (SD +/- 3.17) seconds for the FINGO group. Similarly, both groups demonstrated a slight reduction of 0.3 (SD +/- 0.8) and 0.1 (SD +/- 0.8) in the theta value at the NIH Toolbox Standing Balance Test over 12 months. Regarding 9-HPT, we observed a reduction of 0.51 seconds (SD +/- 3.08) in CLAD patients and an increase of 1.21 seconds (SD +/- 3.66) in FINGO

patients. These longitudinal changes were not statistically significant and did not differ between study groups.

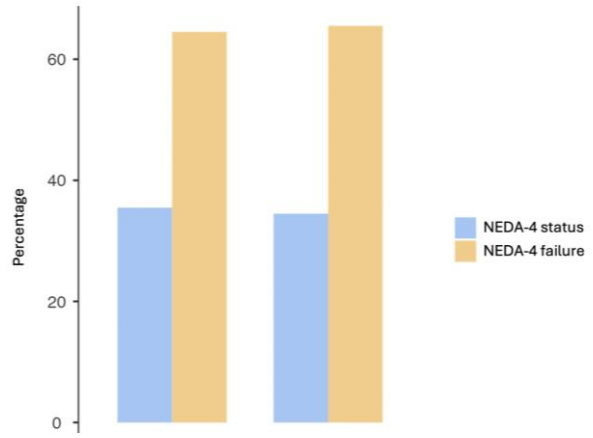

Figure 1: percentage of patients with manteinance of NEDA-4

The percentage of patients with PBVC <-0.4% was 41.9% (13 patients) and 37.9% (11 patients), respectively. The number of patients who maintained NEDA-4 at 12 months was 11 for CLAD patients and 10 for FINGO patients (Figure 1).

Retinal thinning over FU was similar between patients treated with cladribine (pRNFL: -1.6 +/- 3.2 µm; GCIPL: -1.6 +/- 2.5µm) and fingolimod (pRNFL: -1.3 +/- 1.7µm; GCIPL: -0.71 +/- 2 µm). Figure 1 reports the delta of GCIPL and pRNFL over 12 months of the two treatment groups.

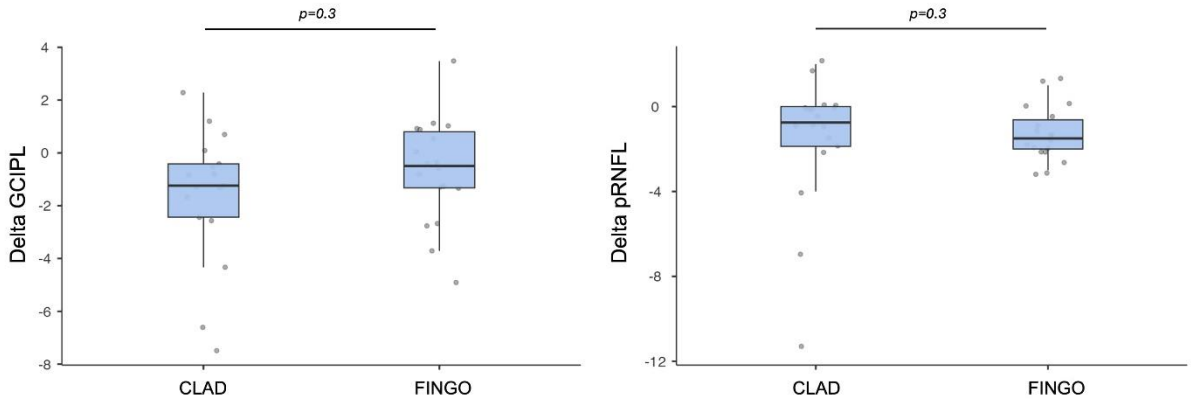

Figure 2.. OCT metrics changes. pRNFL= peripapillary retinal nerve fiber; GCIPL= ganglion cell + inner plexiform layers; CLAD=cladribine; FINGO=fingolimod

Moreover, we observed a substantial stability ICVF and ODI measures within the corpus callosum; ICVF increased by 0.003 in both groups, while ODI increased by 0.002 in both groups. Figure 2 reports representative ICVF and ODI

maps from 2 patients, with the mean values within the corpus callosum of the study groups at baseline and after 12 months.

No additional adverse events related to the two drugs were observed.

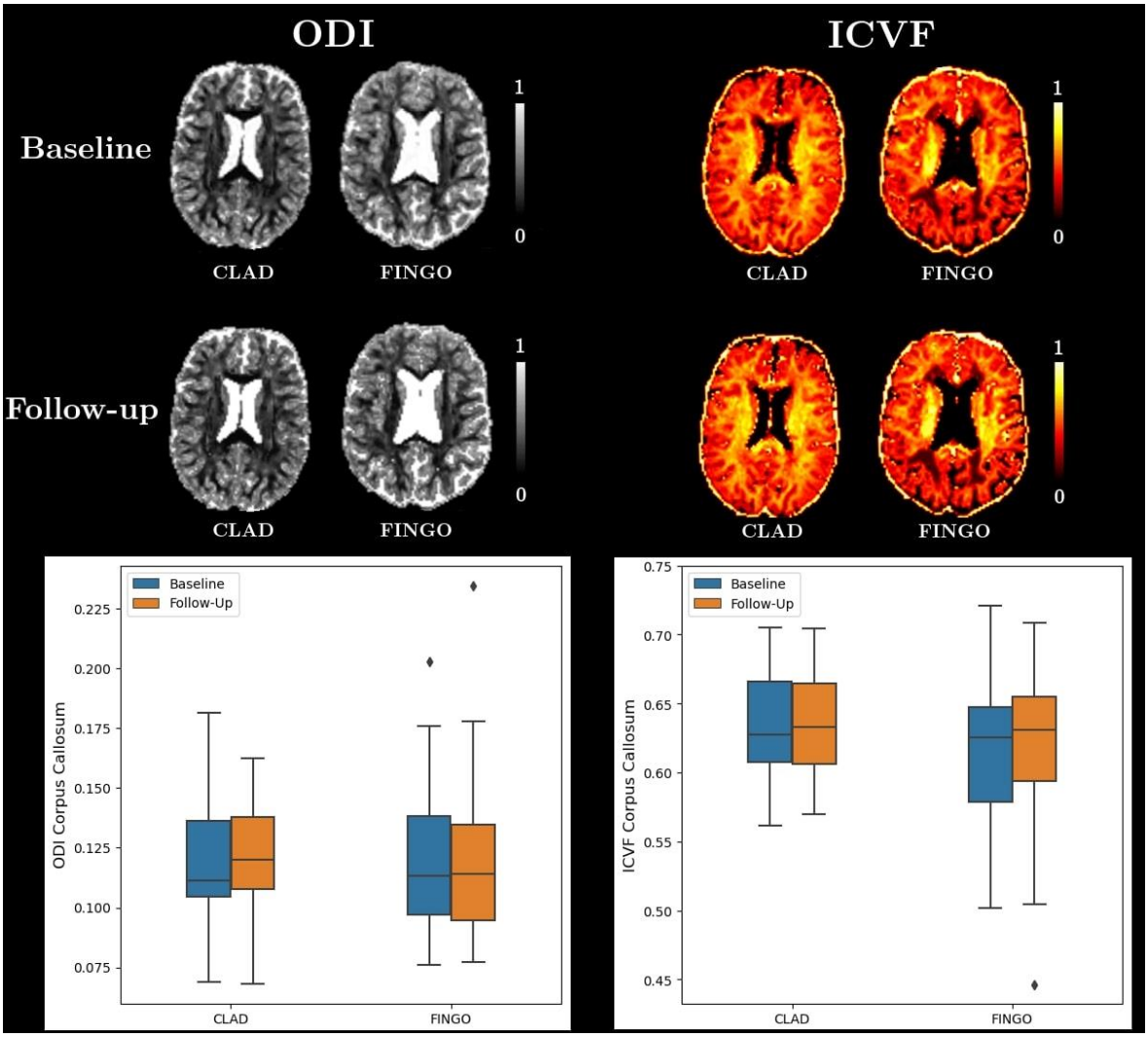

Figure 3. NODDI microstructural changes within the corpus callosum. ODI= Orientation Dispersion Index. ODI quantifies the dispersion of neural fiber orientations in a brain region, indicating how fibers align or spread; ICVF= Intra-Cellular Volume Fracti

4. Second axis. The role of a combined OCT-MRI approach in evaluating neurodegeneration and inflammation in a cohort of patients with MS treated with ocrelizumab.

4.1 Materials and methods

4.1.1 Study design

In this single-center longitudinal observational study, we prospectively included 96 RRMS patients starting ocrelizumab treatment at the MS Center of the University of Genoa, IRCCS Ospedale Policlinico San Martino. Inclusion criteria were: (I) age 18-70 years (II) RRMS diagnosis according to the 2017 McDonald's criteria (III) EDSS score ≤ 7 (III) baseline MRI and OCT assessment within 90 days distance from commencement of ocrelizumab treatment. Exclusion criteria were: (I) other neurological comorbidities, (II) contraindications to MRI, (III) substantial ophthalmological pathologies (including iatrogenic optic neuropathy/diabetes/uncontrolled hypertension), (IV) refractive errors +/− 6-diopters.

Ocrelizumab was prescribed and administered by the treating physician according to regulatory policies. Demographic and clinical characteristic were collected at baseline. All patients were clinically evaluated every 6 months. In order to assess the "no evidence of disease activity" (NEDA-3) criteria during follow-up (FU), information regarding occurrence of clinical relapses, radiological activity (new T2 and/or Gd enhancing lesions), and disability progression (1.5 point increase in EDSS score if baseline EDSS was 0; ≥1.0 point increase if baseline EDSS was between 1.0 and 5.5; ≥ 0.5-point increase if baseline EDSS was ≥ 6) were collected. All patients underwent 3T-MRI with at baseline and at 24-months FU. Due to the concomitant COVID-19 pandemic n=19 patients could not undergo a research MRI at 12-months FU; thus, the 12-months FU MRI is available for a

subset of n=73 patients. A sub-group (n=63 patients) patients underwent spectral-domain (SD)-OCT at baseline.

Another subgroup of patients (n=58), underwent, beyond OCT and collection of demographic and clinical data, assessment of chronic active lesions using QSM at baseline. A follow-up OCT, conducted at least one year after baseline, was also analyzed. All participants provided consent to use their medical history for publication.

4.1.2 MRI protocol, processing and analysis

Subjects were scanned with a 3T MAGNETOM Prisma scanner (Erlangen, Germany) with a 64-channel head and neck coil. The MRI protocol included:

- 3D sagittal T2-FLAIR (176 slices, repetition time/inversion time/echo time (TR/TI/TE): 5,000/1,800/393 ms; resolution 0.4 × 0.4 × 1 mm3);
- 3D sagittal T1 MPRAGE (208 slices, TR/TI/TE: 2,300/919/2.96 ms; resolution 1 × 1 × 1 mm3);
- 3D sagittal-segmented echo-planar-imaging (EPI) (TR/TE 64ms/35ms; Flip Angle=10°; resolution 0.65x0.65x0.65 mm^3) providing signal magnitude and phase.

Careful visual inspection of all MRI images was performed by expert neurologist in field of neuro-radiology, to ensure high image quality. MS lesions were longitudinally segmented on FLAIR and T1-weighted images separately using a semi-automated segmentation technique based on browser user-supervised local thresholding (SinLab, SienaImaging). After denoising (using the nucorrection util, part of FreeSurfer, https://surfer.nmr.mgh.harvard.edu/) and lesion-filling (using FMRIB Software Library -FSL-, https://fsl.fmrib.ox.ac.uk/) of the 3D-T1-weighted MPRAGE, total brain, grey matter, white matter and cerebrospinal fluid were segmented in all patients using the longitudinal pipeline implemented in CAT12, part of SPM12 (http://www.neuro.uni-jena.de/cat/). The derived patient-specific half-way space image obtained by registering all the timepoints into a common space was saved for all subjects. Cortical lobar GM segmentation according to the Desikan-Killiany atlas was obtained using FreeSurfer (https://surfer.nmr.mgh.harvard.edu/) at each timepoint. For all MRIs, thalami and

the other subcortical nuclei were segmented with FIRST, part of FSL (https://fsl.fmrib.ox.ac.uk/)[71]. 3D-T1 images were then normalized to the MNI152 standard space (https://nist.mni.mcgill.ca/atlases/) and to the half-way space using nonlinear registrations with Advanced Normalization Tools (ANTs) 2.3 (http://stnava.github.io/ANTs/). The derived transformations were combined to register all segmented regions from native space to MNI and to the half-way space. Each processing step was visually checked by expert neurologists and corrected if necessary.

For the substudy, as in a previous work from our group[72] FLAIR images and FLAIR lesion masks were aligned to quantitative susceptibility mapping (QSM) and susceptibility map weighted imaging (SMWI) images generated from 3D EPI using a custom set of codes in MATLAB (MathWorks) with STI Suite routines (https://people.eecs.berkeley.edu/~chunlei.liu/software.html) for image phase-unwrapping, background phase removal, and dipole deconvolution. Lesions <0.03 mL and confluent lesions were excluded from the analysis. Two independently trained neurologists with over five years of experience in MS neuroimaging visually classified each MS lesions. In case of disagreement, a consensus was reached upon re-evaluation. According to current guidelines, lesions exhibiting an hyperintense rim compared to the lesion centre were classified as PRLs [72] and lesions with equal QSM intensity compared the background were classified as isointense lesions (ISO) [73].

4.1.3 OCT

For this study, we used the same protocol of the first study. Compared to the first study, however, the thickness of the INL layer was also measured, in addition to that of the pRNFL and GCIPL. As for the first work, in patients with previous unilateral optic neuritis (ON) (n = 23, none occurring during the previous 12 months), only the nonaffected eye was analyzed. Patients with previous bilateral ON were excluded (n=3). Scans violating international-consensus quality-control criteria (OSCAR-IB) were excluded (n=1 baseline scan and n=6 FU scans were

excluded due to poor OCT quality). Finally, n=59 patients with OCT scans were included at baseline and n=53 at 24-months FU.

Regarding the substudy, patients with bilateral optic neuritis (2 patients), and those with OCT follow-up intervals of less than one year (1 patient) were excluded from the analysis. So, for this subgroup, we analyzed the data at baseline and follow-up for 55 patients. As for the principal study, in patients with local damage due to previous unilateral ON (13 patients), only the nonaffected eye was analyzed

4.1.4 Aims of the study

The aims of the study were: i) to assess the impact of OCR treatment on whole brain and regional atrophy at 1 and 2 years FU; ii) assess changes in terms of retinal atrophy as measured by OCT metrics at 2 years FU and to investigate their correlation with brain atrophy. For the subgropu we aimed at assessing the role of QSM-identified chronic active lesions in predicting OCT-derived retinal thinning

4.1.5 Statistical analyses

Statistical analyses were performed using Jamovi (v. 2.3.28,https://www.jamovi.org). A two-sided p-value of <0.05 was considered statistically significant. Descriptive statistics are presented as means with standard deviations (SD), medians with interquartile ranges (IQR), or ranges, as appropriate. The Shapiro-Wilk test and visual inspection of histograms were used to assess the distribution of variables. To assess longitudinal changes in MRI metrics (total brain, cortical, and thalamic volumes, all adjusted for total intracranial volume) and OCT metrics (pRNFL, GCIPL, and INL thickness), repeated measures analysis of covariance (RM-ANCOVA) was employed, adjusted for age and sex.

Correlations between MRI and OCT trajectories throughout follow-up were assessed using partial correlation analysis, controlling for age and sex.

Linear mixed models were used to assess differences in OCT values correcting for the effect of baseline PRLs.

4.2 Results

4.2.1 Study population

A total of 96 RRMS enrolled in the present study. Four of them discontinued treatment before the 24-months assessment due to inefficacy (n=1, day 500), thyroid cancer (n=1, day 180), CNS infection (n=1, day 670), serious COVID-19 infection (n=1, day 390). Accordingly, a total of n=92 patients were included in the final analyses. Demographic and disease-related characteristics at ocrelizumab start and clinical data over 24-months FU are reported in Table 1.

63/92 (68.5%) were females with a mean age of 39 years (SD +/- 10.1) and a mean disease duration of 9.8 years (SD +/- 9). At baseline, the EDSS score was 2.5 with a range of 0–7. Notably, MRI activity at baseline or in the previous three months was detected in 70 patients (76.1%) and only 26 patients (28.3%) were treatment-naïve at the time of study enrollment. The mean number of prior disease-modifying therapies (DMTs) was 1.5 (range: 0–7), while the mean T2 lesion volume measured at baseline was 9.92 mL (SD +/- 10.6).

4.2.2 Outcomes over two-year follow-up

Three patients had a single relapse at +27, +42, and +139 days, respectively. At 2 years, disability worsening-free survival was 82.6% and 83.7% of patients were free of MRI activity, with a NEDA-3 percentage of 67.4%. As expected, most of the inflammatory events (either clinical relapses or MRI activity) occurred during the first 12-months of treatment, consisting in n=14 “early inflammatory active” patients. As per disability worsening, most of the events were PIRA (n=13).

Table 1. Population characteristics and conventional outcomes at follow-up

Population characteristics	OCR Treated Patients (n=92)
Female, n (%)	63 (68.5)
Mean (SD) age, y	39.0 (10.1)
Mean (SD) disease duration, y	9.8 (9.0)
Median (range) baseline EDSS score	2.5 (0–7)
MRI activity at baseline, n (%)*	70 (76.1)
Naive patients, n (%)	26 (28.3)
Mean (range) number of previous DMTs	1.5 (0–7)
Mean (SD) T2 lesion volume, ml	9.92 (10.6)
Conventional outcomes	
Median (range) 1° year EDSS score	2.5 (1–7)
Median (range) 2° year EDSS score	2.5 (1–7)
Relapses over 2-years FU, n (%)	3 (3.3)
Disease progression over 2-years FU, n (%)	16 (17.4)
MRI activity over 2-years FU, n (%)	15 (16.3)
NEDA3 maintenance over 2-years FU, n (%)	62 (67.4)
Early inflammatory activity, n (%)**	14 (15.2)
PIRA, n (%)	13 (14.1)

*MRI activity during the 3 months preceding OCR start; **Relapses and/or MRI activity occurring during the first 12-months of treatment

4.2.3 Effects of ocrelizumab on brain atrophy and retinal layers

Table 2 (A) reports the values of total brain volume, cortical volume, and thalamic volume at baseline and follow-up. Table 2 (B), on the other hand, reports the thickness of the retinal layers (pRNFL, GCIPL, INL) at baseline and follow-up. No statistically significant differences were observed, either in terms of brain or retinal atrophy.

Table 2

A	MRI metrics (n=87)		
	Baseline	**24-months FU**	**p-value***
Total brain volume, ml	1099.61 (125.52)	1097.88 (125.60)	0.739
Cortical volume, ml	464.74 (49.60)	462.64 (51.94)	0.611
Thalamic volume, ml	14.01 (2.29)	13.88 (2.26)	0.803
B	**OCT metrics (n=53)**		
	Baseline	**24-months FU**	**p-value***
pRNFL thickness, µm	97.16 (11.94)	95.93 (12.26)	0.566
GCIPL thickness, µm	81.13 (10.24)	80.46 (10.61)	0.432
INL thickness, µm	36.88 (3.47)	36.61 (3.30)	0.839

4.2.4 Baseline and follow up correlations between retinal layers and brain atrophy

At baseline, we found a statistically significant correlation between baseline GCIPL thickness and both total brain volume and thalamic volume (Image 1). No statistical difference was observed between other retinal layers (pRNFL and INL) and brain atrophy metrics.

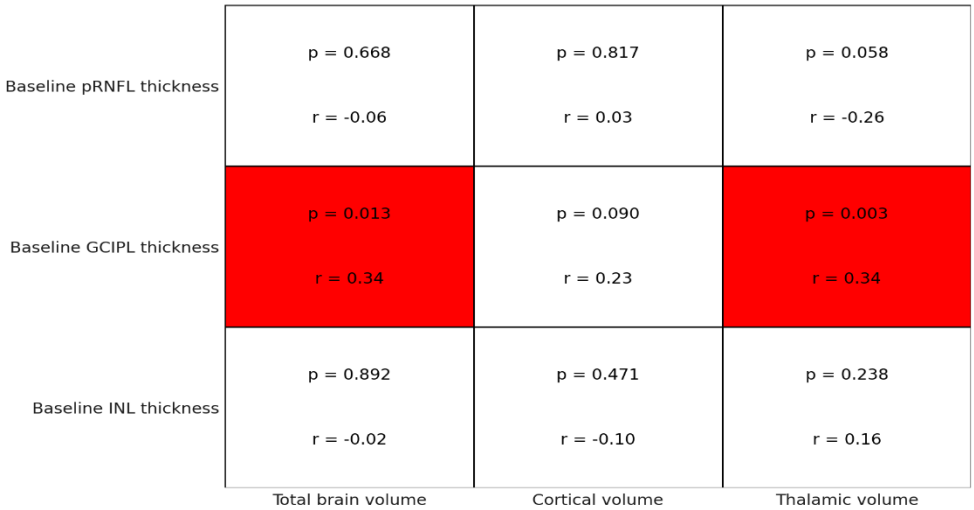

Image 2: correlations between baseline brain atrophy and OCT metrics. P=p-value; r=correlation coefficient

At follow-up (n=53), we observed a statistically significant correlation between GCIPL atrophy and total brain, cortical, and thalamic atrophy (Image 2). No significant correlations were observed between GCIPL/INL and brain atrophy

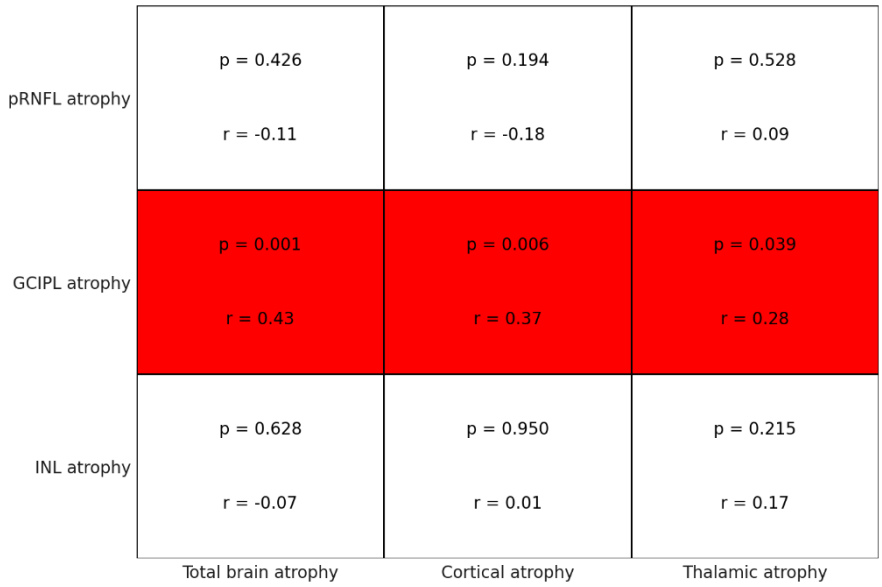

Image 3:correlations between brain and retinal atrophy over 2-years FU

4.2.5 Chronic active lesions and OCT

We analyzed a total of 55 patients. The mean age of the cohort was 37.97 years (SD +/- 14.45). Out of the total, 39 patients (70.91%) were females. The mean disease duration was 6.23 years (SD +/- 7.19). The mean baseline EDSS was 2.32, ranging from 1.0 to 7.0. Regarding disease-modifying therapies (DMTs), 3 were on first-line DMTs, and 52 were on second-line DMTs.

At baseline, the mean RNFL thickness was 98.34 µm (SD +/- 10.48), and the mean GCIPL thickness was 83.39 µm (SD +/- 10.59). 33 patients (60%) had, at baseline, at least one paramagnetic lesion. The mean number of PRLs was 1.53 (range 0-12). Table 3 lists the number of lesions per patient.

Table 3

Number of PRL	Frequency	Percentage
0	22	40.0%
1	14	25.5%
2	9	16.4%
3	4	7.3%
4	2	3.6%
6	1	1.8%
7	2	3.6%
12	1	1.8%

The mean OCT follow-up interval was 2.70 years (SD +/- 1.16). At follow-up, the mean RNFL thickness was 97.88 µm (SD +/-11.03), and the mean GCIPL thickness was 82.77 µm (SD +/-10.82). The mean EDSS at follow-up was 2.23, ranging from 0.0 to 7.0.

Thus, between baseline and follow-up, we observed a minimal reduction in RNFL (0.45 µm) and GCIPL thicknesses (0.30 µm), which was not statistically significant (p-value respectively of 0.131 and 0.521), and a substantial stability in EDSS (an increase of 0.09 points, p-value 0.267).

Moreover, we did not find a statistically significant association between the presence of paramagnetic lesions at baseline and the risk of pRNFL thinning (Image 3) or GCIPL thinning (Image 4).

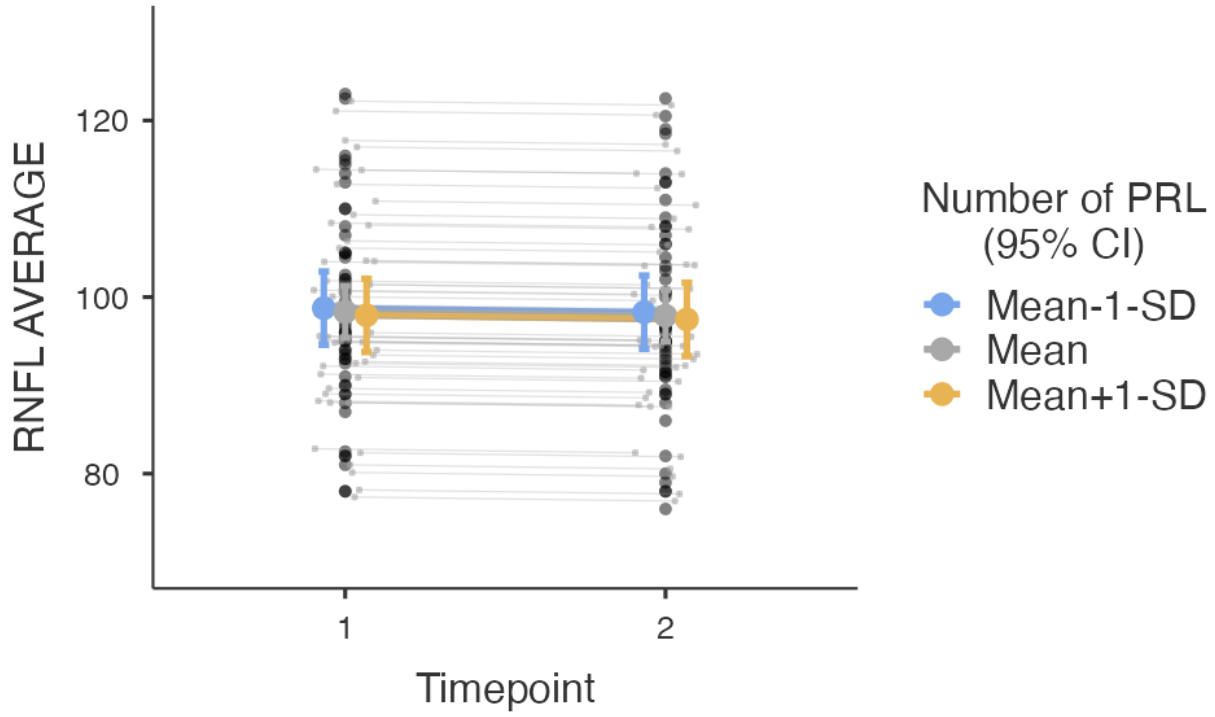

Image 3: Regression model evaluating RNFL thickness changes between baseline and follow-up in patients grouped by PRL presence.

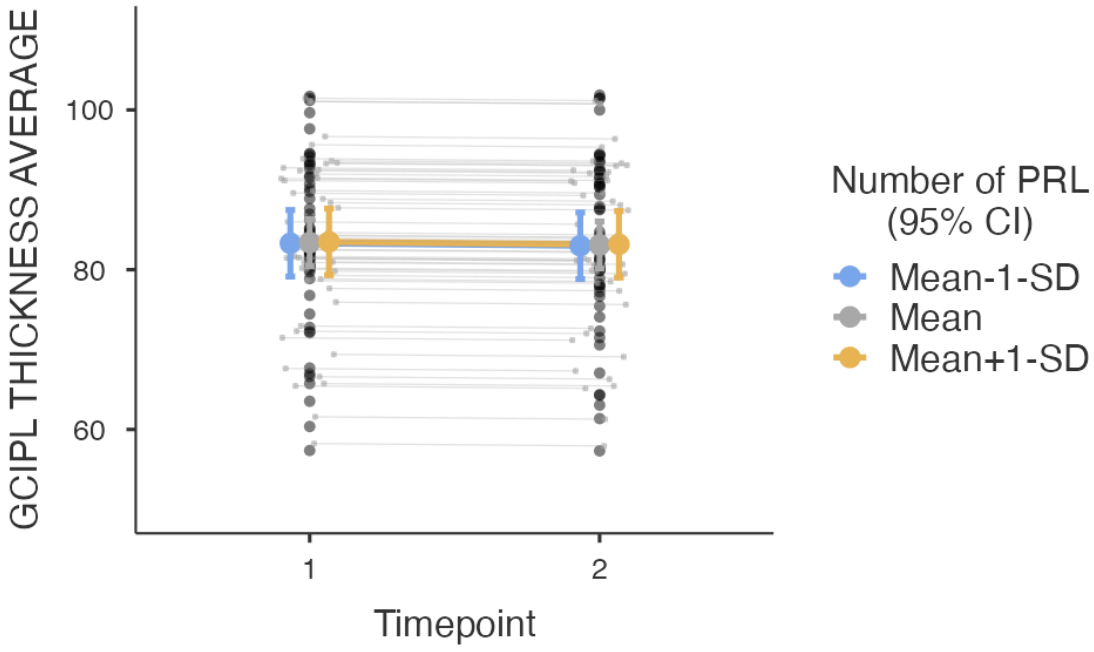

Image 4: Regression model evaluating GCIPL thickness changes between baseline and follow-up in patients grouped by PRL presence.

5. Discussion

In these studies, we aimed to demonstrate that a multimodal approach, incorporating OCT and advanced MRI biomarkers, can assist clinicians in assessing treatment response, including the speed of action of treatments

In the first study, we demonstrated that two DMTs with different mechanisms of action—an antimetabolite and a sequestering agent—achieve comparable efficacy as early as one year after treatment initiation. This was made possible by integrating conventional outcomes, namely NEDA-3, with advanced biomarkers, such as NODDI of the corpus callosum, brain atrophy, and OCT.

Specifically, NODDI serves as a biomarker that provides an almost “in vivo” documentation of the structural disorganization caused by the disease. In this regard, the stability of ICVF and ODI parameters in both groups reflects substantial preservation of intracellular volume and axonal dispersion, respectively—parameters that are potentially compromised during disease course.

The difference between the proportion of patients maintaining NEDA-3 (76.92%) and those achieving NEDA-4 (36.92%)—consistent with findings in the literature—emphasizes the critical role of neurodegeneration and its biomarker, brain atrophy. However, it is important to note that no re-baseline MRI was performed, meaning that the observed brain volume loss at follow-up could be overestimated due to higher baseline activity, a phenomenon known as pseudoatrophy[17].

Another biomarker we utilized was OCT. Using this modality, we observed slight thinning of both RNFL and GCIPL, with no statistically significant differences between the two groups. In this study, we did not perform direct correlations between OCT and other neuroradiological biomarkers.

In the second study, we similarly demonstrated the efficacy of a high-efficacy therapy, beyond conventional biomarkers, using an established neurodegeneration

biomarker—brain atrophy—and OCT. In particular, the near-complete stabilization of retinal and brain volumes highlights the remarkable efficacy of ocrelizumab in counteracting the neurodegenerative processes induced by the disease, in addition to its already well-established effectiveness in addressing the inflammatory component of the pathology.

Moreover, the correlation between GCIPL thinning and brain volumes, both at baseline and follow-up, highlights the relationship of this retinal layer with the neurodegenerative process.

This finding aligns with literature emphasizing the stronger correlation of GCIPL, compared to RNFL, with brain atrophy and its superior ability to identify patients with a progressive disease phenotype. Furthermore, GCIPL appears to be more closely associated with cognitive performance[74]. Conversely, the INL, in our second study not correlate with atrophy metrics, appears to be associated with the inflammatory/acute component of the disease[75]. This was evidenced by its increased thickness in patients not only with recent optic neuritis but also with recent inflammatory activity in general.

This attempt to define the histopathological significance of individual retinal layers is crucial for understanding which aspect of the disease is reflected by retinal layer thinning. For this reason, in the substudy of the second study, we aimed to investigate whether there was a correlation between a marker of smouldering inflammation—paramagnetic rim lesions (PRLs)—and the risk of retinal layer thinning. We did not observe statistically significant differences between the cohort of patients with PRLs and those without PRLs. Unlike the findings of Kranjc et al., this suggests a lack of a definitive correlation between OCT findings and smouldering MS, highlighting the complexity of OCT's relationship with this aspect of the disease.

6. Conclusions

The use of OCT, a readily executable examination with reproducible results, combined with MRI biomarkers, provides the multiparametric approach demanded by the complexity of MS. Clarifying the pathophysiological significance of retinal thinning and the thinning of individual layers will be essential to determine whether this biomarker is complementary to, or redundant with, corresponding neuroradiological biomarkers of neurodegeneration, inflammation, or smouldering MS.

7. References

1. Lublin FD, Reingold SC, Cohen JA, et al. Defining the clinical course of multiple sclerosis: The 2013 revisions. *Neurology*. 2014;83(3):278-286. doi:10.1212/WNL.0000000000000560

2. McDonnell GV, Hawkins SA. Clinical study of primary progressive multiple sclerosis in Northern Ireland, UK. *Journal of Neurology, Neurosurgery & Psychiatry*. 1998;64(4):451-454. doi:10.1136/jnnp.64.4.451

3. Salter A, Thomas NP, Tyry T, Cutter GR, Marrie RA. A contemporary profile of primary progressive multiple sclerosis participants from the NARCOMS Registry. *Mult Scler*. 2018;24(7):951-962. doi:10.1177/1352458517711274

4. Filippi M, Bar-Or A, Piehl F, et al. Multiple sclerosis. *Nat Rev Dis Primers*. 2018;4(1):43. doi:10.1038/s41572-018-0041-4

5. Reich DS, Lucchinetti CF, Calabresi PA. Multiple Sclerosis. Longo DL, ed. *N Engl J Med*. 2018;378(2):169-180. doi:10.1056/NEJMra1401483

6. Kappos L, Wolinsky JS, Giovannoni G, et al. Contribution of Relapse-Independent Progression vs Relapse-Associated Worsening to Overall Confirmed Disability Accumulation in Typical Relapsing Multiple Sclerosis in a Pooled Analysis of 2 Randomized Clinical Trials. *JAMA Neurol*. 2020;77(9):1132. doi:10.1001/jamaneurol.2020.1568

7. Giovannoni G, Popescu V, Wuerfel J, et al. Smouldering multiple sclerosis: the 'real MS.' *Ther Adv Neurol Disord*. 2022;15:17562864211066751. doi:10.1177/17562864211066751

8. Levin M, Gardner L, Douglas J, Meyers L, Lee S, Shin Y. Neurodegeneration in multiple sclerosis involves multiple pathogenic mechanisms. *DNND*. Published online March 2014:49. doi:10.2147/DNND.S54391

9. Caranova M, Soares JF, Batista S, Castelo-Branco M, Duarte JV. A systematic review of microstructural abnormalities in multiple sclerosis detected with NODDI and DTI models of diffusion-weighted magnetic resonance imaging. *Magnetic Resonance Imaging*. 2023;104:61-71. doi:10.1016/j.mri.2023.09.010

10. Seyedmirzaei H, Nabizadeh F, Aarabi MH, Pini L. Neurite Orientation Dispersion and Density Imaging in Multiple Sclerosis: A Systematic Review. *Magnetic Resonance Imaging*. 2023;58(4):1011-1029. doi:10.1002/jmri.28727

11. Schneider T. Sensitivity of multi-shell NODDI to multiple sclerosis white matter changes: a pilot study. *FN*. 2017;32(2):97. doi:10.11138/FNeur/2017.32.2.097

12. Granberg T, Fan Q, Treaba CA, et al. In vivo characterization of cortical and white matter neuroaxonal pathology in early multiple sclerosis. *Brain*. 2017;140(11):2912-2926. doi:10.1093/brain/awx247

13. Storelli L, Pagani E, Meani A, Preziosa P, Filippi M, Rocca MA. Advanced diffusion-weighted imaging models better characterize white matter neurodegeneration and clinical outcomes in multiple sclerosis. *J Neurol*. 2022;269(9):4729-4741. doi:10.1007/s00415-022-11104-z

14. Preziosa P, Pagani E, Meani A, et al. NODDI, diffusion tensor microstructural abnormalities and atrophy of brain white matter and gray matter contribute to cognitive impairment in multiple sclerosis. *J Neurol*. 2023;270(2):810-823. doi:10.1007/s00415-022-11415-1

15. Battaglini M, Gentile G, Luchetti L, et al. Lifespan normative data on rates of brain volume

changes. *Neurobiology of Aging*. 2019;81:30-37. doi:10.1016/j.neurobiolaging.2019.05.010

16. De Stefano N, Stromillo ML, Giorgio A, et al. Establishing pathological cut-offs of brain atrophy rates in multiple sclerosis. *J Neurol Neurosurg Psychiatry*. Published online April 22, 2015:jnnp-2014-309903. doi:10.1136/jnnp-2014-309903

17. Samia K, Rohit B. Cerebral pseudoatrophy or real atrophy after therapy in multiple sclerosis. *Annals of Neurology*. 2010;68(6):778-779. doi:10.1002/ana.22254

18. Cagol A, Schaedelin S, Barakovic M, et al. Association of Brain Atrophy With Disease Progression Independent of Relapse Activity in Patients With Relapsing Multiple Sclerosis. *JAMA Neurol*. 2022;79(7):682. doi:10.1001/jamaneurol.2022.1025

19. on behalf of the MAGNIMS study group, Sastre-Garriga J, Pareto D, et al. MAGNIMS consensus recommendations on the use of brain and spinal cord atrophy measures in clinical practice. *Nat Rev Neurol*. 2020;16(3):171-182. doi:10.1038/s41582-020-0314-x

20. Rocca MA, Horsfield MA, Sala S, et al. A multicenter assessment of cervical cord atrophy among MS clinical phenotypes. *Neurology*. 2011;76(24):2096-2102. doi:10.1212/WNL.0b013e31821f46b8

21. Oh J, Sotirchos ES, Saidha S, et al. Relationships between quantitative spinal cord MRI and retinal layers in multiple sclerosis. *Neurology*. 2015;84(7):720-728. doi:10.1212/WNL.0000000000001257

22. Kappos L, De Stefano N, Freedman MS, et al. Inclusion of brain volume loss in a revised measure of 'no evidence of disease activity' (NEDA-4) in relapsing–remitting multiple sclerosis. *Mult Scler*. 2016;22(10):1297-1305. doi:10.1177/1352458515616701

23. Kuhlmann T, Ludwin S, Prat A, Antel J, Brück W, Lassmann H. An updated histological classification system for multiple sclerosis lesions. *Acta Neuropathol*. 2017;133(1):13-24. doi:10.1007/s00401-016-1653-y

24. Prineas JW, Kwon EE, Cho E, Sharer LR. Continual Breakdown and Regeneration of Myelin in Progressive Multiple Sclerosis Plaquesa. *Annals of the New York Academy of Sciences*. 1984;436(1):11-32. doi:10.1111/j.1749-6632.1984.tb14773.x

25. Maggi P, Sati P, Nair G, et al. Paramagnetic Rim Lesions are Specific to Multiple Sclerosis: An International Multicenter 3T MRI Study. *Annals of Neurology*. 2020;88(5):1034-1042. doi:10.1002/ana.25877

26. Absinta M, Sati P, Masuzzo F, et al. Association of Chronic Active Multiple Sclerosis Lesions With Disability In Vivo. *JAMA Neurol*. 2019;76(12):1474. doi:10.1001/jamaneurol.2019.2399

27. Britze J, Frederiksen JL. Optical coherence tomography in multiple sclerosis. *Eye*. 2018;32(5):884-888. doi:10.1038/s41433-017-0010-2

28. Parisi V, Manni G, Spadaro M, et al. Correlation between morphological and functional retinal impairment in multiple sclerosis patients. *Invest Ophthalmol Vis Sci*. 1999;40(11):2520-2527.

29. Ikuta F, Zimmerman HM. Distribution of plaques in seventy autopsy cases of multiple sclerosis in the United States. *Neurology*. 1976;26(6_part_2):26-28. doi:10.1212/WNL.26.6_Part_2.26

30. Evangelou N. Size-selective neuronal changes in the anterior optic pathways suggest a differential susceptibility to injury in multiple sclerosis. *Brain*. 2001;124(9):1813-1820. doi:10.1093/brain/124.9.1813

31. Ciccarelli O, Toosy AT, Hickman SJ, et al. Optic radiation changes after optic neuritis detected by tractography-based group mapping. *Human Brain Mapping*. 2005;25(3):308-316. doi:10.1002/hbm.20101

32. Adams N. *ATLAS OF OCT: Retinal Anatomy in Health & Pathology*. https://media.heidelbergengineering.com/downloads/ebooks/303019-003_SPECTRALIS_Book_Adams-Atlas-of-OCT_US.pdf

33. Costello F, Coupland S, Hodge W, et al. Quantifying axonal loss after optic neuritis with optical coherence tomography. *Annals of Neurology*. 2006;59(6):963-969. doi:10.1002/ana.20851

34. Kupersmith MJ, Garvin MK, Wang JK, Durbin M, Kardon R. Retinal ganglion cell layer thinning within one month of presentation for optic neuritis. *Mult Scler*. 2016;22(5):641-648. doi:10.1177/1352458515598020

35. Mateo J, Esteban O, Martínez M, Grzybowski A, Ascaso FJ. The Contribution of Optical Coherence Tomography in Neuromyelitis Optica Spectrum Disorders. *Front Neurol*. 2017;8:493. doi:10.3389/fneur.2017.00493

36. Bennett J, De Seze J, Lana-Peixoto M, et al. Neuromyelitis optica and multiple sclerosis: Seeing differences through optical coherence tomography. *Mult Scler*. 2015;21(6):678-688. doi:10.1177/1352458514567216

37. Bernard JT, Romero R, Agrawal K, Jager R, Rezania K. Optical coherence tomography in Susac's syndrome. *Multiple Sclerosis and Related Disorders*. 2014;3(1):110-116. doi:10.1016/j.msard.2013.05.005

38. Pakeerathan T, Havla J, Schwake C, et al. Rapid differentiation of MOGAD and MS after a single optic neuritis. *J Neurol*. 2024;271(11):7222-7231. doi:10.1007/s00415-024-12666-w

39. Vidal-Jordana A, Pareto D, Cabello S, et al. Optical coherence tomography measures correlate with brain and spinal cord atrophy and multiple sclerosis disease-related disability. *Euro J of Neurology*. 2020;27(11):2225-2232. doi:10.1111/ene.14421

40. Walter SD, Ishikawa H, Galetta KM, et al. Ganglion Cell Loss in Relation to Visual Disability in Multiple Sclerosis. *Ophthalmology*. 2012;119(6):1250-1257. doi:10.1016/j.ophtha.2011.11.032

41. Saidha S, Syc SB, Durbin MK, et al. Visual dysfunction in multiple sclerosis correlates better with optical coherence tomography derived estimates of macular ganglion cell layer thickness than peripapillary retinal nerve fiber layer thickness. *Mult Scler*. 2011;17(12):1449-1463. doi:10.1177/1352458511418630

42. Lampert EJ, Andorra M, Torres-Torres R, et al. Color vision impairment in multiple sclerosis points to retinal ganglion cell damage. *J Neurol*. 2015;262(11):2491-2497. doi:10.1007/s00415-015-7876-3

43. Seay M, Fan Y, Bermel R. Ocular Coherence Tomography Macular Volume Predicts Walking Speed in Patients with Multiple Sclerosis (P6.305). *Neurology*. 2016;86(16_supplement):P6.305. doi:10.1212/WNL.86.16_supplement.P6.305

44. Mirmosayyeb O, Zivadinov R, Weinstock-Guttman B, Benedict RHB, Jakimovski D. Optical coherence tomography (OCT) measurements and cognitive performance in multiple sclerosis: a systematic review and meta-analysis. *J Neurol*. 2023;270(3):1266-1285. doi:10.1007/s00415-022-11449-5

45. Toledo J, Sepulcre J, Salinas-Alaman A, et al. Retinal nerve fiber layer atrophy is associated

with physical and cognitive disability in multiple sclerosis. *Mult Scler*. 2008;14(7):906-912. doi:10.1177/1352458508090221

46. Martinez-Lapiscina EH, Arnow S, Wilson JA, et al. Retinal thickness measured with optical coherence tomography and risk of disability worsening in multiple sclerosis: a cohort study. *The Lancet Neurology*. 2016;15(6):574-584. doi:10.1016/S1474-4422(16)00068-5

47. Rothman A, Murphy OC, Fitzgerald KC, et al. Retinal measurements predict 10-year disability in multiple sclerosis. *Ann Clin Transl Neurol*. 2019;6(2):222-232. doi:10.1002/acn3.674

48. Zimmermann HG, Knier B, Oberwahrenbrock T, et al. Association of Retinal Ganglion Cell Layer Thickness With Future Disease Activity in Patients With Clinically Isolated Syndrome. *JAMA Neurol*. 2018;75(9):1071. doi:10.1001/jamaneurol.2018.1011

49. Costello F, Hodge W, Pan YI, Freedman M, DeMeulemeester C. Differences in retinal nerve fiber layer atrophy between multiple sclerosis subtypes. *Journal of the Neurological Sciences*. 2009;281(1-2):74-79. doi:10.1016/j.jns.2009.02.354

50. Oberwahrenbrock T, Schippling S, Ringelstein M, et al. Retinal Damage in Multiple Sclerosis Disease Subtypes Measured by High-Resolution Optical Coherence Tomography. *Multiple Sclerosis International*. 2012;2012:1-10. doi:10.1155/2012/530305

51. Henderson APD, Trip SA, Schlottmann PG, et al. An investigation of the retinal nerve fibre layer in progressive multiple sclerosis using optical coherence tomography. *Brain*. Published online December 4, 2007:awm285. doi:10.1093/brain/awm285

52. Button J, Al-Louzi O, Lang A, et al. Disease Modifying Therapies Modulate Retinal Atrophy in Multiple Sclerosis: A Retrospective Study (S45.008). *Neurology*. 2016;86(16_supplement):S45.008. doi:10.1212/WNL.86.16_supplement.S45.008

53. Saidha S, Al-Louzi O, Ratchford JN, et al. Optical coherence tomography reflects brain atrophy in multiple sclerosis: A four-year study. *Annals of Neurology*. 2015;78(5):801-813. doi:10.1002/ana.24487

54. Cagol A, Fuertes NC, Stoessel M, et al. Optical coherence tomography reflects clinically relevant gray matter damage in patients with multiple sclerosis. *J Neurol*. 2023;270(4):2139-2148. doi:10.1007/s00415-022-11535-8

55. Ong YT, Hilal S, Cheung CY, et al. Retinal neurodegeneration on optical coherence tomography and cerebral atrophy. *Neuroscience Letters*. 2015;584:12-16. doi:10.1016/j.neulet.2014.10.010

56. Chalkias E, Topouzis F, Tegos T, Tsolaki M. The Contribution of Ocular Biomarkers in the Differential Diagnosis of Alzheimer's Disease versus Other Types of Dementia and Future Prospects. *JAD*. 2021;80(2):493-504. doi:10.3233/JAD-201516

57. Krajnc N, Dal-Bianco A, Leutmezer F, et al. Association of paramagnetic rim lesions and retinal layer thickness in patients with multiple sclerosis. *Mult Scler*. 2023;29(3):374-384. doi:10.1177/13524585221138486

58. Iaffaldano P, Lucisano G, Butzkueven H, et al. Early treatment delays long-term disability accrual in RRMS: Results from the BMSD network. *Mult Scler*. 2021;27(10):1543-1555. doi:10.1177/13524585211010128

59. Thompson AJ, Banwell BL, Barkhof F, et al. Diagnosis of multiple sclerosis: 2017 revisions of the McDonald criteria. *The Lancet Neurology*. 2018;17(2):162-173. doi:10.1016/S1474-4422(17)30470-2

60. Kurtzke JF. Rating neurologic impairment in multiple sclerosis: An expanded disability status scale (EDSS). *Neurology*. 1983;33(11):1444-1444. doi:10.1212/WNL.33.11.1444

61. Feys P, Lamers I, Francis G, et al. The Nine-Hole Peg Test as a manual dexterity performance measure for multiple sclerosis. *Mult Scler*. 2017;23(5):711-720. doi:10.1177/1352458517690824

62. Kalinowski A, Cutter G, Bozinov N, et al. The timed 25-foot walk in a large cohort of multiple sclerosis patients. *Mult Scler*. 2022;28(2):289-299. doi:10.1177/13524585211017013

63. Peller A, Garib R, Garbe E, et al. Validity and reliability of the NIH Toolbox® Standing Balance Test As compared to the Biodex Balance System SD. *Physiotherapy Theory and Practice*. 2023;39(4):827-833. doi:10.1080/09593985.2022.2027584

64. Gaser C, Dahnke R, Thompson PM, Kurth F, Luders E, Alzheimer's Disease Neuroimaging Initiative. *CAT – A Computational Anatomy Toolbox for the Analysis of Structural MRI Data*. Neuroscience; 2022. doi:10.1101/2022.06.11.495736

65. Tournier JD, Smith R, Raffelt D, et al. MRtrix3: A fast, flexible and open software framework for medical image processing and visualisation. *NeuroImage*. 2019;202:116137. doi:10.1016/j.neuroimage.2019.116137

66. Sacco S, Caverzasi E, Papinutto N, et al. Neurite Orientation Dispersion and Density Imaging for Assessing Acute Inflammation and Lesion Evolution in MS. *AJNR Am J Neuroradiol*. 2020;41(12):2219-2226. doi:10.3174/ajnr.A6862

67. MRI Atlas of Human White Matter. AJNR Am J Neuroradiol. 2006 Jun;27(6):1384–5. PMCID: PMC8133945.

68. Avants BB, Tustison NJ, Song G, Cook PA, Klein A, Gee JC. A reproducible evaluation of ANTs similarity metric performance in brain image registration. *NeuroImage*. 2011;54(3):2033-2044. doi:10.1016/j.neuroimage.2010.09.025

69. Cruz-Herranz A, Balk LJ, Oberwahrenbrock T, et al. The APOSTEL recommendations for reporting quantitative optical coherence tomography studies. *Neurology*. 2016;86(24):2303-2309. doi:10.1212/WNL.0000000000002774

70. Schippling S, Balk L, Costello F, et al. Quality control for retinal OCT in multiple sclerosis: validation of the OSCAR-IB criteria. *Mult Scler*. 2015;21(2):163-170. doi:10.1177/1352458514538110

71. Patenaude B, Smith SM, Kennedy DN, Jenkinson M. A Bayesian model of shape and appearance for subcortical brain segmentation. *NeuroImage*. 2011;56(3):907-922. doi:10.1016/j.neuroimage.2011.02.046

72. Tazza F, Boffa G, Schiavi S, et al. Multiparametric Characterization and Spatial Distribution of Different MS Lesion Phenotypes. *AJNR Am J Neuroradiol*. 2024;45(8):1166-1174. doi:10.3174/ajnr.A8271

73. Bagnato F, Sati P, Hemond CC, et al. Imaging chronic active lesions in multiple sclerosis: a consensus statement. *Brain*. 2024;147(9):2913-2933. doi:10.1093/brain/awae013

74. Dreyer-Alster S, Gal A, Achiron A. Optical Coherence Tomography Is Associated With Cognitive Impairment in Multiple Sclerosis. *Journal of Neuro-Ophthalmology*. 2022;42(1):e14-e21. doi:10.1097/WNO.0000000000001326

75. Balk LJ, Coric D, Knier B, et al. Retinal inner nuclear layer volume reflects inflammatory disease activity in multiple sclerosis; a longitudinal OCT study. *Multiple Sclerosis Journal -*

Experimental, Translational and Clinical. 2019;5(3):2055217319871582. doi:10.1177/2055217319871582